Surface structure analysis of Ni(111)-$(\sqrt{3}\times\sqrt{3})R30°$-Pb by impact-collision ion-scattering spectroscopy

Kenji Umezawa, Shigemitsu Nakanishi, and Takahiro Yumura
Department of Physics, University of Osaka Prefecture, Sakai, Osaka 599-8531, Japan

Walter M. Gibson
Department of Physics, University at Albany, SUNY, 1400 Washington Avenue, Albany, New York 12222

Masatoshi Watanabe and Yoshiaki Kido
Department of Physics, Ritsumeikan University, Kusatsu, Shiga 525-0055, Japan

Shunya Yamamoto, Yasushi Aoki, and Hiroshi Naramoto
Department of Materials Development, Japan Atomic Energy Research Institute, Takasaki, Gunma 370-1207, Japan
(Received 30 December 1996; revised manuscript received 4 June 1997)

Impact-collision ion-scattering spectroscopy, low-energy electron diffraction, and Rutherford backscattering spectroscopy have been used to analyze the Ni{111}-$(\sqrt{3}\times\sqrt{3})R30°$-Pb structure. It was found that annealing Pb-covered Ni surfaces with an initial coverage of 0.45 ML gives rise to a stable Ni{111}-$(\sqrt{3}\times\sqrt{3})R30°$-Pb structure. The experimental data and computer simulations support a structural model for the Ni{111}-$(\sqrt{3}\times\sqrt{3})R30°$-Pb structure in which Pb atoms displace part of the first layer Ni atoms and incorporate them into the first Ni layer, with the Pb atoms displaced outward 0.2 Å with respect to the first-layer Ni atoms. However, 20–30% of Pb atoms are randomly missing from the ideal Ni{111}-$(\sqrt{3}\times\sqrt{3})R30°$-Pb model. This study shows surface alloying of immiscible metals in agreement with other recent studies. [S0163-1829(97)00340-8]

I. INTRODUCTION

The investigation of metal-on-metal overlayer systems is an interesting and important subject for understanding surface-related phenomena such as catalytic reactions and surface specific compound formation.[1–3] The Stranski-Krastanov growth mode is common for metal on metal systems when deposition occurs at a low temperature or when the components exhibit little tendency for alloy formation.[1] However in many systems it is of interest to consider the possibility of bulk or surface alloy formation. If the constituent metals have dissimilar sizes but tend to form strongly ordered intermetallic phases, such a phase may be nucleated at the surface or an overlayer of unique structure may be formed. In recent studies, elements which are immiscible in the bulk have been found to form stable two-dimensional mixtures at the surface.[4–6] These studies include Alkali-metal adsorbates on Al(111) and (001), Au on Ni(110), and Ag on Pt(111), respectively. Related theoretical work was proposed by Tersoff as well.[7]

In a continuation of previous work,[8] we found that upon annealing the Rb-Ni(111) system to 600 °C, the surface tends to equilibrate at a $(\sqrt{3}\times\sqrt{3})R30°$ structure if sufficient Pb is present. The Pb/Ni(111) phase has an atomic size mismatch; the nearest-neighbor distances of Pb and Ni are 3.5 and 2.49 Å, respectively.[9] This paper reports results of our studies of a Ni(111)-$(\sqrt{3}\times\sqrt{3})R30°$-Pb structure by low-energy impact-collision ion-scattering spectroscopy (ICISS) combined with low-energy electron diffraction (LEED) and MeV ion scattering. We conclude that this $(\sqrt{3}\times\sqrt{3})R30°$ structure shows surface-confined alloy formation in immiscible systems. ICISS has been used in a number of cases to study clean, reconstructed, and adsorbate covered solid surfaces.[2,10–12] The surface structure can be determined directly in real space by analyzing the angular anisotropy ion-scattering intensities. In the present study, the structure of the Pb-Ni(111) surface was studied by observing shadowing and blocking of low-energy 3-keV-Ne^+ ions, and the results indicate that some of the Pb atoms are incorporated into the first Ni layer, but with the Pb displaced slightly outward. The absolute amount of Pb adsorption onto Ni(111) was obtained from Rutherford backscattering spectroscopy (RBS) measurements using 2-MeV-He^+ ions.

We used two types of ion-scattering analysis programs for comparison with experimental data: (1) the calculations for the three-dimensional cross section for ions that scatter sequentially and classically from two atoms, and are computationally very fast[13,14] and (2) molecular-dynamics simulations involving many target atoms.[15–17] In principle, trajectory calculations based on molecular dynamics are more realistic, but the amount of computer time required to accumulate a statistically significant data set is prohibitive. In practice, such calculations are time consuming for determining the ICISS angular dependence. We have mainly determined the surface structure by using the first way. Calculation results based on molecular-dynamics simulations support the surface structures determined by the calculations for the three-dimensional cross section. In this paper, intensities shown by experimental and simulation data are compensated for the area exposed to the incident beams and normalized by multiplying by the cosine of the polar angle.

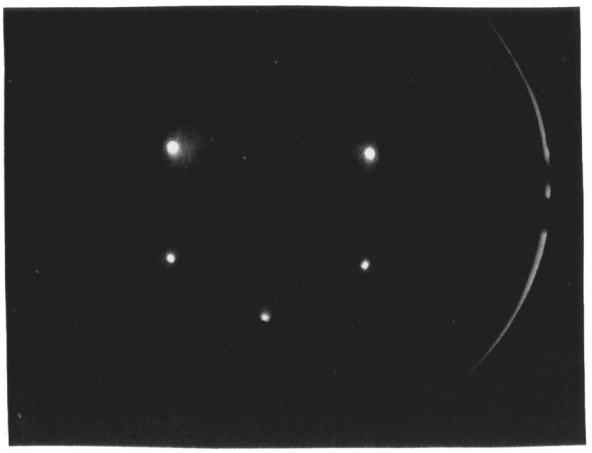

(a)

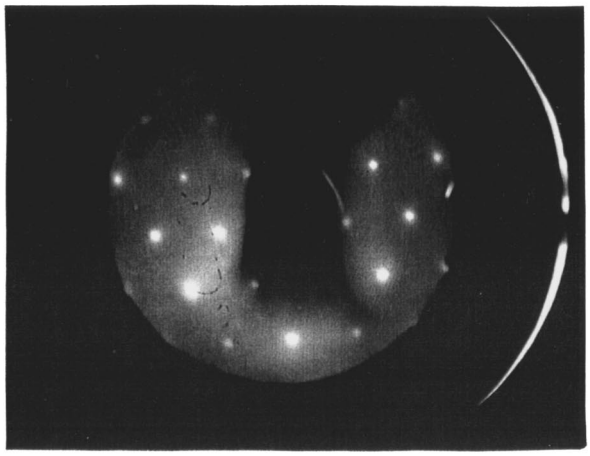

(b)

FIG. 1. LEED patterns (125 eV) taken from (a) clean Ni{111}(1×1) and (b) Ni{111}-$(\sqrt{3}\times\sqrt{3})R30°$-Pb.

II. EXPERIMENTAL PROCEDURES

The experimental procedures described here were performed in an ultrahigh vacuum system with LEED, Auger electron spectroscopy (AES), and ICISS facilities. The base pressure during the experiment was maintained below 5×10^{-8} Pa. A Ni(111) substrate ($\phi12\times0.5\,\mathrm{mm}^2$ thickness) was mechanically and electrochemically polished. After the crystal was mounted on a standard UHV-XYZ manipulator, it was extensively cleaned *in situ* by repeated cycles of 500-eV-Ar^+ bombardment and subsequent annealing at 700 °C to remove the surface damage. The state of the surface was monitored by AES, LEED, and ICISS measurements. Sharp (1×1) LEED patterns were thus obtained as shown in Fig. 1(a) and the cleanliness of the surface was confirmed by AES and ICISS, which is sensitive to surface contamination. Lead was evaporated at a rate of about 0.03 ML/min onto the Ni(111) crystal to a coverage of 0.45 ML at room temperature, then annealed at a substrate temperature of 600 °C. The Ni(111)-$(\sqrt{3}\times\sqrt{3})R30°$-Pb LEED patterns were finally observed after cooling of the substrate to room temperature as shown on Fig. 1(b).

The ICISS spectra were taken by chopping the primary 3-keV-Ne^+ beam and detecting 180° backward-scattered particles after free flight through a drift tube of 60 cm by means of a microchannel plate detector which was coaxially mounted along the primary tube. Polar angle scans were performed from $-85°$ to $+85°$ in 1° increments with an average beam current of 3–5 pA. Also, the Pb coverage at the completion of the $(\sqrt{3}\times\sqrt{3})R30°$ structure was verified by RBS measurements using 2-MeV-He^+ ions.

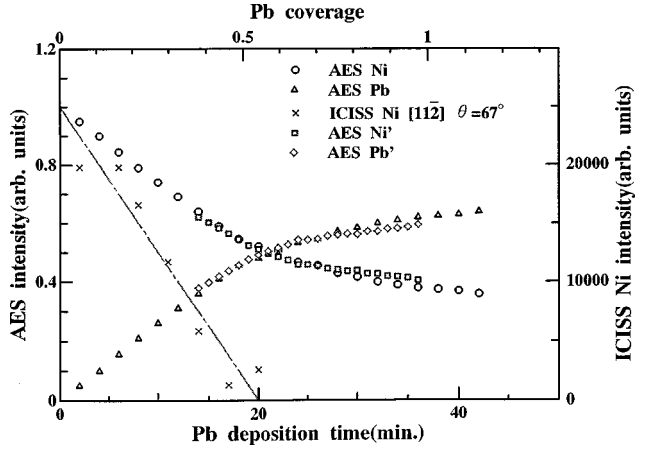

FIG. 2. Lead on nickel Auger intensities and a variation in nickel ICISS intensity as a function of Pb deposition on Ni(111). The symbols of (○), (△), and (×) were obtained from the Pb deposition at room temperature. The symbols of (◇) and (□) were obtained from the Pb deposition at room temperature after forming the $(\sqrt{3}\times\sqrt{3})R30°$ structure.

III. RESULTS AND DISCUSSION

In AES measurements, the Ni(61 eV) and the Pb(94 eV) Auger peak intensities were monitored during Pb deposition. Figure 2 shows the variation of the $I_{\mathrm{Ni}}/(I_{\mathrm{Ni}}+I_{\mathrm{Pb}})$ and $I_{\mathrm{Pb}}/(I_{\mathrm{Ni}}+I_{\mathrm{Pb}})$ signal intensities as a function of Pb deposition time and includes results from the previous (Ref. 8) as well as the present study. Both the Pb and Ni AES curves show a change of slope at about the same coverage (time). The attenuation of the Ni signals obtained from ICISS goes to zero at a deposition time of 20 min. We assumed that the Pb deposition rate is constant and linear in time. It was concluded in the previous study that the coverage obtained after 20 min of Pb deposition corresponds to completion of the first layer coverage.[8] Also, a Pb Auger intensity from the $(\sqrt{3}\times\sqrt{3})R30°$ structure following the annealing which corresponds to 1/3 ML for an ideal structure is almost in agreement with the experimental value of Pb surface density, 5.4×10^{14} atoms/cm^2 or 0.29 ± 0.03 ML obtained from RBS measurements using a 2-MeV-He^+ ion beam. [One monolayer is defined as 1.86×10^{15} atoms cm^{-2} from the ideal Ni density in a (111) plane of a bulk crystal.] It shows that of the 0.45 ML of Pb deposited on the sample, about 0.16 ML disappeared from the surface upon annealing the substrate at 600 °C. For additional Pb deposition at room temperature after completion of the $(\sqrt{3}\times\sqrt{3})R30°$ structure, the Pb and Ni AES curves followed closely the AES curves obtained from Pb deposition at room temperature. In fact, as before, the structure changed into the previously observed $(4\times4)'$ structure at a net coverage of 0.54 ML. The $(4\times4)'$ structure means that it is close to the ideal 4×4 structure, but the measured lead-lead spacing of 3.39 Å is 6% larger than that

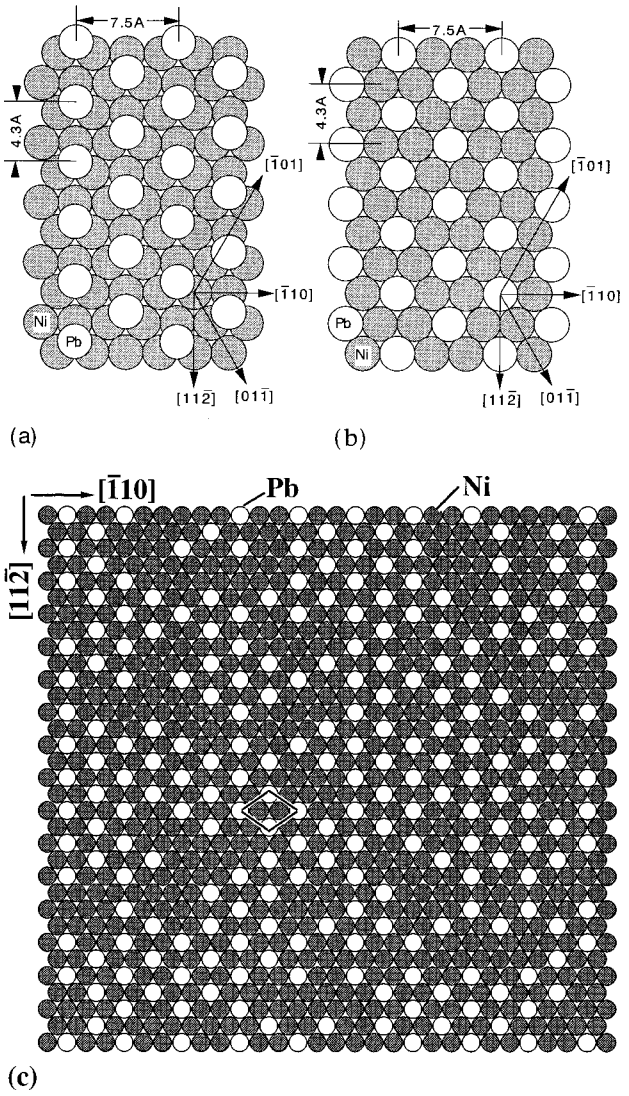

FIG. 3. Ball models showing (a) Pb-overlayer, (b) Pb-incorporated, and (c) partial of Pb incorporation with $(\sqrt{3}\times\sqrt{3})R30°$ ordering [around 30% of Pb atoms are missing to the ideal structural model (b)]. Solid lines show the unit mesh of the $(\sqrt{3}\times\sqrt{3})R30°$ structure.

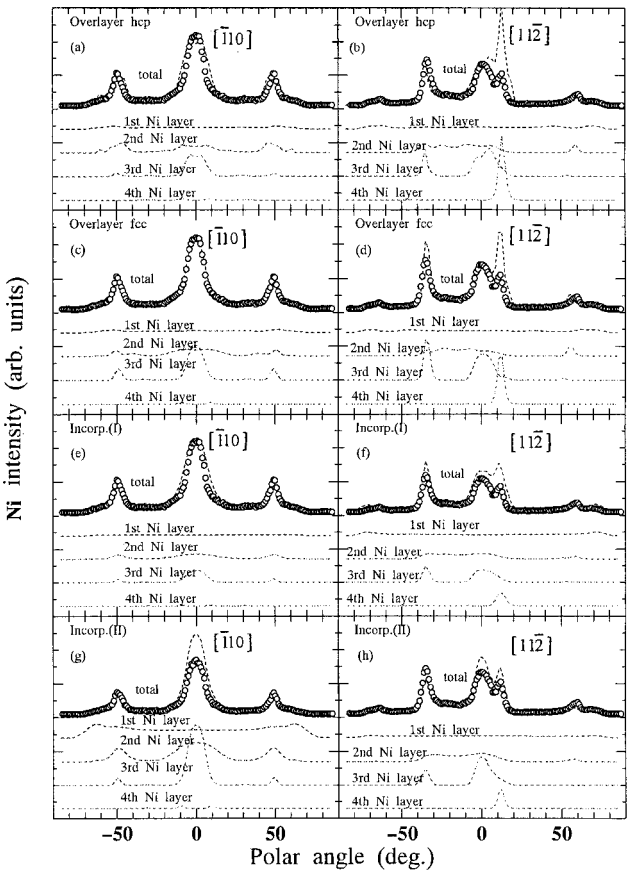

FIG. 4. A series of ICISS polar angle scans and computer simulations for 3-keV-Ne^+ ions backscattered from Ni atoms along the [110] [(a) hcp overlayer, (c) fcc overlayer, (e) incorporated, and (g) partial Pb incorporation] and [112] azimuths [(b) hcp overlayer, (d) fcc overlayer, (f) incorporated, and (h) a partial Pb incorporation]. Incorp. (I) and (II) correspond to the surface structural models shown in Fig. 3(b) and Fig. 6, respectively. Circles and the broken curves show the experimental-data and computer simulations, respectively.

of 3.24 Å in the ideal bulk structure. This $(4\times4)'$ structure was the same structure as we observed by Pb deposition at room temperature in the previous work.[8] This phenomenon implies that the Pb atoms do not grow as an overlayer structure on the $(\sqrt{3}\times\sqrt{3})R30°$ structure. (This is an interesting phenomenon but we will not discuss it in this paper.)

The $(\sqrt{3}\times\sqrt{3})R30°$ LEED pattern observed for the annealed Pb/Ni(111) suggests structures such as those shown in Figs. 3(a) and 3(b) in which the symmetry of the LEED pattern is determined by the arrangement of the Pb atoms either as an overlayer or incorporated into the surface. In considering overlayer structures the most likely adsorption sites for the Pb are the threefold hollows, either the hcp sites (Pb atom directly above a second-layer Ni atom) or the fcc sites (Pb atom directly above a third-layer Ni atom). To distinguish between an overlayer (hcp or fcc) model [Fig. 3(a)] and an incorporated model [Fig. 3(b)], in which the Pb replaces Ni atoms, it is necessary to more carefully examine the incidence angle dependence of the scattered signals coming from the Pb and the Ni atoms by ICISS. To clarify whether the Pb is present as an overlayer in hcp, fcc sites or is incorporated into the lattice, computer simulations were compared with experimental data. Figure 4 shows the intensity of the ICISS spectra of $(\sqrt{3}\times\sqrt{3})R30°$ for ions scattered from Ni as a function of polar angle along [110] and [112] azimuths. The dashed curves are obtained from computer simulations based on a hcp-overlayer model [Figs. 4(a) and 4(b)], a fcc-overlayer model [Figs. 4(c) and 4(d)], an incorporated model [Figs. 4(e) and 4(f)], and a partly incorporated model [Figs. 4(g) and 4(h)].[13,14] The computer simulations were carried out by using a Thomas-Fermi-Moliere scattering potential with an adjustable parameter C; 0.9 for Pb and 0.7 for Ni atoms to fit the experimental results, respectively. This adjustable parameter C does not appear in the theory of the screening length proposed by Frisov,[18] but has been proposed by numerous researchers to improve agreement with experimental results and is discussed in detail elsewhere.[19] Along the [110] azimuth, the calculated results agree well with experimental data for all of the models investigated. It shows that polar angle dependence is not so sensitive to the structure differences along this azimuth. The peaks at $\pm50°$ come from multiple focusing effects due to the out-of-

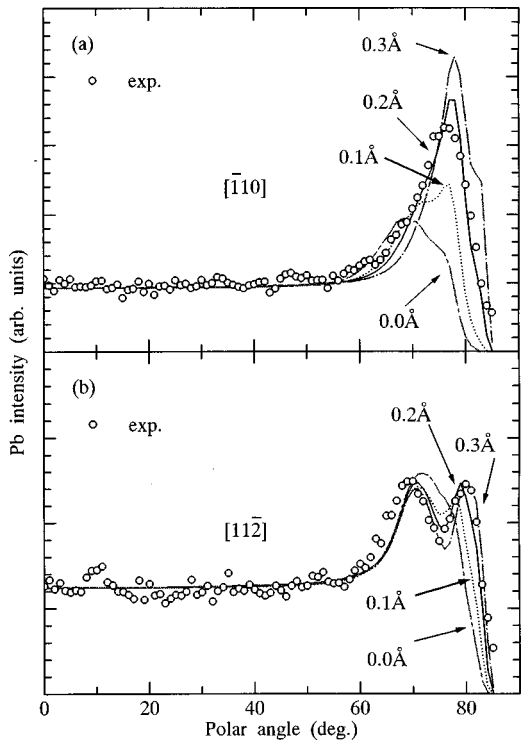

FIG. 5. A series of ICISS polar angle scans and computer simulations for 3-keV-Ne^+ ions backscattered from Pb atoms along the (a) [110] and (b) [112] azimuths. Circles and the broken curves show the experimental data and computer simulations based on the model shown in Fig. 3(c), respectively. The other model structures [Figs. 3(a) and 3(b)] would show only single Pb scattering peaks along [112] the azimuth.

plane scattering by second- and third-layer Ni atoms. Also the peak at 0° comes from third-layer Ni atoms due to focusing effects. On the other hand, along the [112] azimuth, the Ni peaks at $-45°$ show signals coming from the third-layer Ni atoms. Other peaks at 0° and 12° come from the third- and fourth-layer Ni atoms due to focusing effects. However calculated Ni peak intensities at 12° in both the hcp [Fig. 4(b)] and fcc [Fig. 4(d)] overlayer structures are much stronger than that of experimental data. In an ideal incorporated model [Fig. 3(b)], the calculated Ni peak intensities are closer but still higher than the experimental value as shown in Fig. 4(f).

The intensity of ions scattered from Pb as a function of polar angle is shown in Fig. 5. In Fig. 5(a), surface Pb peak can be only seen at 78° in the [110] azimuth. However, along the [112] azimuth shown in Fig. 5(b), two Pb signal peaks were observed at 72° and 81°. The presence of two peaks indicates that more than one Pb spacing exists along the [112] direction. [In the ideal structure model shown in Fig. 3(b), a single peak is predicted along both azimuths, because one Pb spacing only exist.] Therefore, another structure model needs to be examined as shown in Fig. 3(c). In this structure model about 30% of the Pb atoms corresponding to an ideal $\sqrt{3}\times\sqrt{3}$ structure are randomly missing and the remaining Pb is incorporated into the first Ni layer. Some different types of Pb spacing randomly exist; 4.3, 8.6, and 12.9 Å, etc. along the [112] azimuth, respectively. Other different Pb spacings, 7.5 and 15.0 Å, etc., exist in the [110] azimuth as well. In Fig. 5, lines represent the calculated Pb intensity depending on the Pb height from 0.0 to 0.3 Å above the center-of-mass position of the first layer of Ni atoms. In Fig. 5(a) the calculated curve for the Pb height of 0.0 Å, which corresponds to the ideal coplanar, is inconsistent with the experimental data in the [110] azimuth. For this case the peak at around 70° on the calculated curve is due to focusing effects of the nearest-neighbor Ni atoms since both Pb and Ni atoms have the same height. Also for this case, a double peak is not predicted in the [112] azimuth. This height shows that the focusing effects of the nearest-neighbor Ni atoms for Pb atoms are more effective than the focusing effects between Pb atoms. Therefore the calculated data are inconsistent with the experimental data. However, at a Pb displacement of 0.2 Å with respect to the first Ni layer, calculated curves nicely fit the Pb polar scattering peak positions observed along both azimuths as shown in Fig. 5. Especially, double peaks are clearly observed in the [112] azimuth. The calculated critical angles for different Pb spacings, 4.3, 8.6, and 12.9 Å correspond to 72.7°, 80.7°, and 81.9°, respectively. These calculations indicate that triple peaks are predicted over the polar angle of 70° in the [112] azimuth. In practice, it is hard to distinguish the small-angle difference between 80.7° and 81.9° because of the thermal broadening of the peaks. This is the reason why experimental data show only double peaks along this direction. A similar thing is seen in the [110] azimuth. A wide single peak in this azimuth is mainly due to focusing effects between Pb atoms as well as Ni-Pb atoms. Since Pb atoms have an outward displacement of 0.2 Å with respect to the first Ni layer, the focusing effects of Ni atoms for Pb atoms are less evident. The critical angles of the different Pb spacings, 7.5 Å, and 15.0 Å correspond to calculated angles of 77.8° and 82.2°, respectively. The number of Pb atoms with spacing of 15.0 Å is smaller than those with spacing of 7.5 Å. It is thus hard to see double peaks in the experimental data as shown in Fig. 5(a). However, such an angle difference makes a wide single peak. Furthermore, in this model the calculated Ni intensity is almost in agreement with the experimental data as shown in Figs. 4(g) and 4(h). These examinations show that Pb atoms have the height of 0.2 Å above the center of mass position of the first layer of Ni atoms. The model of Fig. 3(c) is an example in order to explain the experimental data, but this model involves a random defect of around 30% of the Pb atoms corresponding to an ideal $\sqrt{3}\times\sqrt{3}$ structure.

In addition, we show the calculated results of the molecular-dynamics simulations in Fig. 6. In these calculations, 20% of the Pb atoms are randomly missing. One can see that the calculated data are in agreement with the experimental data in the [11$\bar{2}$] azimuth. The molecular-dynamics simulations also support the conclusion that some Pb atoms are missing from the ideal $\sqrt{3}\times\sqrt{3}$ structure. The Pb coverage of 0.29 ± 0.03 ML obtained from RBS measurements is almost in good agreement with 0.26 ML of Pb atoms corresponding to 20% of missing Pb atoms. The removed Ni atoms may be brought to step or kink sites at the surface. The macroscopic number of step and kink sites is not changed.

The physics behind this surface structure model is that a pair of elements, Pb and Ni, which are immiscible in the bulk, form a mixture confined to a single atomic layer at the surface. The known examples of surface-confined alloys all involve the deposition of a large atom onto a small one:

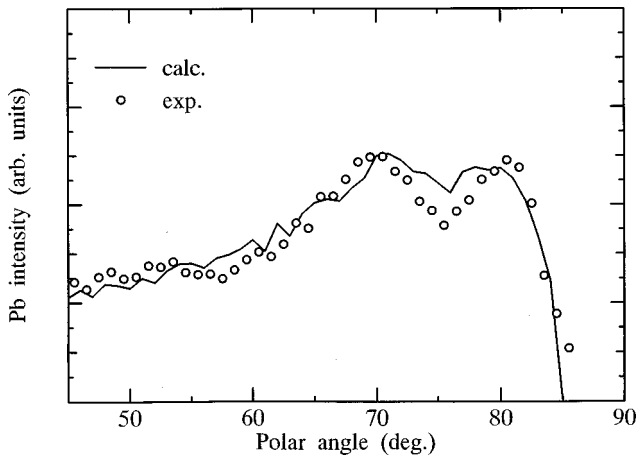

FIG. 6. A series of ICISS polar angle scans and molecular-dynamics simulations for 3-keV-Ne^+ ions backscattered from Ni atoms along the [112] azimuths. 20% of the Pb atoms are missing in these simulations.

alkali metals on Al, Au on Ni, Ag on Pt.[4–6] The Ni-Pb system seems to fit nicely into this category of systems. The Ni(111)-$(\sqrt{3}\times\sqrt{3})R30°$-Pb structure may originate in factors from a correlation of surface energy or surfaces stress with different atomic sizes as Tersoff explained in his theoretical work on the surface-confined alloy formation.[7] However, it is still an open question why this surface alloy forms the ordered structure of $(\sqrt{3}\times\sqrt{3})R30°$.

IV. CONCLUSION

Impact-collision ion-scattering spectroscopy ICISS, LEED, and RBS were applied to analyze the Ni{111}-$(\sqrt{3}\times\sqrt{3})R30°$-Pb structure. It was found that annealing a Pb-covered Ni surface with an initial coverage of 0.45 ML at 600 °C gives rise to a stable Ni{111}-$(\sqrt{3}\times\sqrt{3})R30°$-Pb structure. The experimental data and computer simulations support a structural model for the Ni{111}-$(\sqrt{3}\times\sqrt{3})R30°$-Pb structure in which Pb atoms displace the first-layer Ni atoms and incorporate into the first Ni layer, with an outward displacement of 0.2 Å with respect to the first layer Ni atoms. However, 20–30 % of the Pb atoms are randomly missing from the ideal Ni{111}-$(\sqrt{3}\times\sqrt{3})R30°$-Pb structure. This single-layer surface alloy structure is apparently determined by size mismatch of the Ni and Pb atoms. The survival of this structure during the relatively high annealing temperature of 600 °C anneal is a measure of its stability and indicates strong intermetallic bonding. Such intermetallic surface alloy structures may be dominated by strain effects, e.g., to reduce strain energy at the surface.

[1] E. Bauer, Appl. Surf. Sci. **11/12**, 479 (1982).
[2] Yi-sha ku and S. H. Overbury, Surf. Sci. **273**, 341 (1992).
[3] K. Gürtler and K. Jacobi, Surf. Sci. **134**, 309 (1983).
[4] J. Neugebauer and M. Scheffler, Phys. Rev. Lett. **71**, 577 (1993).
[5] L. P. Nielsen, F. Besenbacher, I. Stensgaard, E. Laesgsgaard, C. Engdahl, P. Stoltze, K. W. Jacobsen, and J. K. Nørskov, Phys. Rev. Lett. **71**, 754 (1993).
[6] H. Röder, R. Schuster, H. Brune, and K. Kern, Phys. Rev. Lett. **71**, 2086 (1993).
[7] J. Tersoff, Phys. Rev. Lett. **74**, 434 (1995).
[8] K. Umezawa, A. Takahashi, T. Yumura, S. Nakanishi, and W. M. Gibson, Surf. Sci. **365**, 118 (1996).
[9] C. Kittel, *Introduction to Solid State Physics*, 7th ed. (Wiley, New York, 1996), p. 24.
[10] M. Aono, C. Ohshima, S. Zaima, S. Otani, and Y. Ishizawa, Jpn. J. Appl. Phys. **20**, L829 (1981).
[11] H. Nius, Nucl. Instrum. Methods Phys. Res. **218**, 230 (1983).
[12] S. Nakanishi, K. Kawamoto, and K. Umezawa, Surf. Sci. **287/288**, 974 (1993).
[13] M. T. Robinson and I. M. Torrens, Phys. Rev. B **9**, 5008 (1974).
[14] R. S. Williams, M. T. Kato, R. S. Daley, and M. Aono, Surf. Sci. **225**, 355 (1990).
[15] Y. Kido and T. Koshikawa, J. Appl. Phys. **67**, 187 (1990).
[16] I. Konomi, A. Kawamoto, and Y. Kido, Surf. Sci. **207**, 427 (1988).
[17] J. Nakata, N. Jourdan, H. Yamaguchi, K. Takahei, Y. Yamamoto, and Y. Kido, J. Appl. Phys. **77**, 3095 (1995).
[18] O. Firsov, Zh. Éksp. Teor. Fiz. **33**, 696 (1958) [Sov. Phys. JETP **6**, 534 (1958)].
[19] S. H. Oberbury and D. R. Huntley, Phys. Rev. B **32**, 6278 (1985).